THE EXPECTED POTENTIAL OF TERRASAR-X HIGH RESOLUTION SPOTLIGHT MODE DATA FOR SHALLOW SEA BOTTOM TOPOGRAPHY IMAGING: A PREVIEW

Ingo Hennings and Dagmar Herbers

Leibniz-Institut für Meereswissenschaften an der Universität Kiel (IFM-GEOMAR), 24148 Kiel, Germany; ihennings(at)ifm-geomar.de

ABSTRACT

An improved radar imaging theory of marine sand wave signatures based on quasi-specular scattering is presented. For quasi-specular scattering from a rough ocean surface, the normalised radar cross section (NRCS) is proportional to the total variance of slopes created by ocean surface waves. Quasi-specular scattering becomes dominant at higher radar frequencies. The formulated theory is applicable to the X-band synthetic aperture radar (SAR) of TerraSAR-X, Germany's first civil national remote sensing satellite realised by a public-private partnership. The improved quasi-scattering theory contains the additional dependences on the up- and crosswind wave slopes, the angle between the upwind and perpendicular current direction to the sand wave crest, and the angle between the radar range direction and the upwind direction. The current-short surface wave interaction is described by weak hydrodynamic interaction theory in the relaxation time approximation. Detailed TerraSAR-X data with a spatial resolution of up to 1 m and up to 1.5 dB radiometric resolution will be used with the advantage to be nearly weather independent. The investigation area is the tidal channel of the Lister Tief in the German Bight of the North Sea characterised by large morphological changes of four-dimensional submarine bedforms in time and space. Due to the high spatial resolution of the TerraSAR-X data it will be possible to identify sea surface roughness variations caused by meso-scale sand waves < 300 m widths at water depths < 40 m and associated unique oceanographic phenomena such as up- and downwelling events, turbulence, and eddies. The proposed measurement configuration and all needed *in situ* data are described. Advanced knowledge of transport characteristics of marine sand waves is very important for ship navigation and coastal zone management.

Keywords: Quasi-specular scattering theory, TerraSAR-X, high resolution spotlight mode, Lister Tief, marine sand waves.

INTRODUCTION

It has been scientifically proved that predicted climate change and related sea-level rise will strongly modify hydro-, sediment- and morphodynamics in coastal zones worldwide. Experts expected that the coastal erosion especially at the German island of Sylt in the North Sea will still be enhanced. The erosion rate depends largely on the frequency and energy of winter storms and on the duration of high water. Beach nourishment is carried out at the northwestern part of Sylt island due to erosion forces. The sand transport is going mainly to northeasterly and easterly directions into the Lister Tief area. Observations show that sand depositions take place at the northern location of Sylt, the western part of the Ellenbogen, and erosion takes place more easterly of the Ellenbogen in the vicinity of lighthouse List East. The shoreline of the Ellenbogen has changed extensively during the last decades (1,2). Sand transport influenced by ocean waves, currents and tides are complex processes. Therefore, research is required on the sources, properties and transport budgets of terrestrial and marine sediments in coastal areas. Basic research is necessary to achieve new insights into wave- and current-induced sand transport over sea beds covered by bedforms such as sand waves. These investigations are important for assimilation of predictive coastal morphological models.

Radar remote sensing techniques have become operationally during the last three decades and have now been established among other observation tools in marine earth sciences. Radar signatures of sea bottom topography are dominated by Bragg scattering since most of the imaging radars operate at incidence angles between 20° and 70° (3). At low radar incidence angles, $< 20°$, quasi-specular scattering is dominating. In addition, quasi-specular scattering becomes dominant at higher radar frequencies. According to Bragg scattering theory, the normalised radar cross section (NRCS) for small water surface waves is proportional to the wave height spectral density at the Bragg backscatter wavenumbers. For quasi-specular scattering from a rough ocean surface, the NRCS is proportional to the total variance of slopes created by ocean surface waves. The radar imaging mechanism of sea bottom topography strongly depends on the radar incidence angle, radar frequency, radar polarisation, current speed and -direction, as well as wind speed and -direction. The most important assumption for the radar imaging mechanism of submarine bedforms is the presence of strong currents, preferably tidal currents ≥ 0.5 m s^{-1} at wind speeds ≤ 8 m s^{-1}. The mathematical formulation of the radar imaging mechanism of the sea bed as well as experimental studies of these phenomena are subjects of several past and present international research activities (4,5,6,7,8,9,10,11,12,13,14,15).

It is commonly known that L- and P-band imaging radar systems are to be most suitable to show radar signatures of the sea bed. On the other hand, data of spaceborne X-band synthetic aperture radar (SAR) systems have not been analysed sufficiently enough within the scientific community. New *in situ* measurements show up- and downwelling phenomena of the three-dimensional current velocity field contributing significantly to the interaction between marine sand waves and the tidal flow, which has not been known before in detail (16). Similar circulation patterns associated with Langmuir supercells off the coast of New Jersey of the eastern U.S. coast have been identified (17). The up- and downwelling regimes cause remarkable depressions at the troughs of sand waves with a maximum depth of 2 m and a width of up to 50 m. These depressions are superimposed with current ripples which are oriented perpendicular to the dominant tidal current direction. It is expected that, at the depressions of the sea bed, so-called waterspouts will be created by the upward orientated component of the three-dimensional current velocity field generating turbulence patterns or boils at the water surface. It is supposed that within the boils enhanced sediment concentration or other water constituents can be observed. Consequently, it is assumed that waterspouts and boils are an additional mechanism for sediment transport in tidal channels and similar shallow environments. They may also be a major trigger of biogeochemical as well as physical processes of shallow seas. The theoretical work of these observations, processes, and interactions is still under development for complete mathematical solutions.

These boils have not been identified with existing spaceborne imaging radars due to their low spatial resolution. But with the launch of TerraSAR-X high resolution spotlight mode this should be possible. In the second section the system is described with a view to a historical airborne SAR image. The goals and work schedule are outlined in the third section. All methods which will be carried out including the study area, TerraSAR-X measurements, *in situ* data as bathymetric, shipborne X-band radar, Acoustic Doppler Current Profiler (ADCP), and meteorological measurements as well as the improved quasi-specular scattering theory are presented in the fourth section. Finally, the last section contains the conclusions.

TERRASAR-X HIGH RESOLUTION SPOTLIGHT MODE

TerraSAR-X is Germany's first civil national remote sensing satellite realised by a public-private partnership between the German Aerospace Center (DLR) and the European Aeronautic Defence and Space Company (EADS) Astrium GmbH. The radar remote sensing satellite has been launched sucessfully at 0214 UT 15 June 2007 on a Russian/Ukrainian DNEPR-1 launch vehicle from the Baikonur cosmodrome in Kazakhstan. An artist's view of TerraSAR-X is shown in Figure 1.
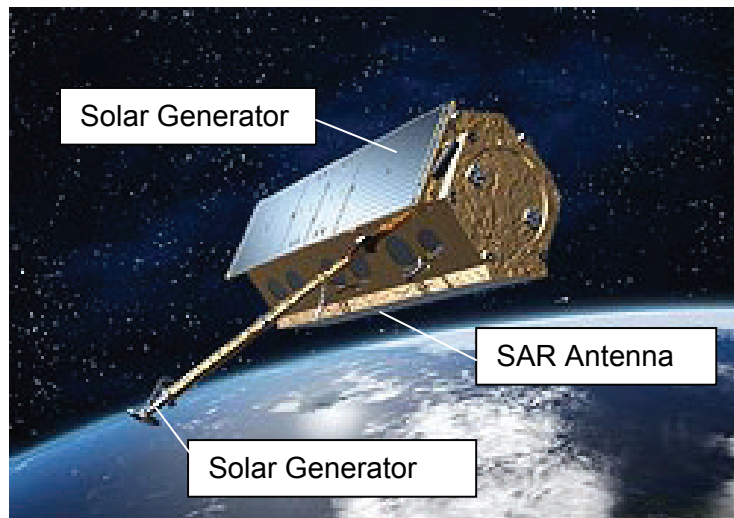
Figure 1: Artist's view of TerraSAR-X (modified source: German Aerospace Center (DLR)).

Table 1: Parameters of TerraSAR-X High Resolution Spotlight Mode.

Parameter	Value
Scene extension	5 km (azimuth) × 10 km (ground range)
Full performance incidence angle range	20° – 55°
Data access incidence angle range	15° – 60°
Number of elevation beams	95 (full performance)
	123 (data access)
Number of azimuth beams	ca. 249
Azimuth steering angle	± 0.75°
Azimuth resolution	1 m (single polarisation)
	2 m (dual polarisation)
Ground range resolution	1.34 m - 3.21 m (at 55°...20° incidence angle)
Polarisations	*HH* or *VV* (single)
	HH / *VV* (dual)

TerraSAR-X is an X-band SAR based on active phased array antenna technology using a radar frequency of 9.65 GHz and a radar wavelength of 3.11 cm. Each pulse can be transmitted either vertically (*V*) or horizontally (*H*) polarised. The backscattered signal can be received with either vertical or horizontal polarisation, independent of the transmit polarisation. Imaging will be possible in single, dual, and quad polarisation (on experimental basis). A very high spatial resolution in the flight or azimuth direction can be achieved if the radar antenna length is short or a spotlight mode is used from the view of sensor technology. Shorter antennas must be larger in the vertical dimension to illuminate the required area, which usually means scanning in elevation to obtain a reasonable swath width. TerraSAR-X is a highly programmable X-band SAR and in the following, a brief description of the innovative spotlight mode sensor technology will be given. The TerraSAR-X spotlight mode allows a very high spatial resolution in azimuth direction. It is based on electrical beam steering in azimuth direction in a way that the same target region is illuminated during the whole data recording period. In this way the illumination time will be increased, the nominal ground velocity of the radar beam is reduced, the size of the synthetic aperture will become larger and with it a high spatial resolution is achieved. Unfortunately, the larger aperture of a high spatial azimuth resolution results at the expense of azimuthal scene size. The TerraSAR-X sensor technology offers high flexibility in order to image the sea area of interest. A number of 123 spotlight elevation beams are defined in order to adjust the scene centre in small increments so that the required area can be placed in the middle of a scene. In azimuth direction about 125 beams from a set of 249

beams are used to extend the synthetic aperture. The imaging process is started and controlled by the Global Positioning System (GPS). This procedure will be activated when TerraSAR-X reaches a position along the orbit that has been calculated from the required scene centre coordinates of the investigated sea area. The TerraSAR-X high resolution spotlight mode (HS) is designed for an azimuth resolution of 1 m resulting in an azimuth scene size of at least 5 km. The characteristic values are given in Table 1.

Historical airborne SAR data

An example of the expected kind of radar data from TerraSAR-X high resolution spotlight mode is shown in Figure 2. This *HH* polarised radar image has been collected by the APD-10 X-band SAR mounted in an F-4 jet aircraft over the sea area of the Lister Tief. Acquisition time was at 0936 UT 27 September 1979 during the Maritime Remote Sensing (MARSEN) experiment. The radar scene of subswath B has a geometrical resolution of 3 m $\times$ 3 m and the mean incidence angle was 72°. These data have been taken 46 minutes before low tide during ebb tidal phase at station List West of the entrance to the Lister Tief. The wind speed was 10 m s^{-1} and the wind direction was from 290°. Although the wind and current conditions were unfavourable for the visibleness of the sea bottom topography several radar signatures caused by submarine sand waves can be identified. The sea area is dominated by bright features of elongated streaks leading to a degraded spatial resolution in the along-track or azimuth direction. This phenomenon is a SAR artifact due to scatterer motion effects. It has been suggested that breaking waves are responsible for such features observed on SAR imagery. Several handheld camera images of breaking waves associated with convergent tidal current regimes over submarine sand waves taken from the water surface in the Lister Tief at moderate to high wind speeds support this statement.

Goals

The overall objective of this project is to demonstrate the high potential of TerraSAR-X data for synoptic mapping of large areas in coastal waters. It is expected that the very high geometric and radiometric resolutions enable very detailed analyses of NRCS modulation signatures caused by current variations and meso-scale dynamics such as boils associated with marine sand waves in tidal channels as the Lister Tief. For the complete analysis and interpretation of TerraSAR-X data the GKSS X-band Radar Doppler Current Profiler (RDCP) system has been adapted for necessary *in situ* measurements of such meso-scale current features interacting with the sea bed. In addition, the NRCS will be also measured by the RDCP system during ebb and flood tidal phases. TerraSAR-X data will be compared with RDCP X-band data under very low grazing angles. This comparison is important for the interpretation of NRCS modulation signatures because vertical (*VV*)-polarised data are available from both radar systems, but the shipborne radar system is a real aperture radar (RAR) and the spaceborne radar system is a SAR imaging the sea surface at different grazing angles. In addition, phase modulation or velocity bunching contributes to the SAR imaging mechanism as a special artifact.

Bathymetric measurements will be taken by a high spatial resolution multibeam echo sounding system quasi simultaneously. The mapping of sea bottom topography from TerraSAR-X data in shallow coastal areas with water depth $\leq$ 50 m will be less cost intensive, always up-to-date, at least available every 11 days and therefore is an innovative new observation configuration for end users managing the coastal zone. Such observation capabilities had not been available before neither from space nor from on board research ships.

To achieve the overall objective, the following aims have to be fulfilled:
- Acquisition of *in situ* data for validation of TerraSAR-X data,
- understanding sea bottom topography signatures at the water surface as a function of time and space using TerraSAR-X data,
- improving the X-band radar imaging theory.

The innovative character of the project can be summarised as:
- The proposed research offers good potentials to apply radar remote sensing techniques for coastal research and management of the coastal zone.

- The project will show advantages and limitations of using radar remote sensing techniques to receive weather-independent synoptic information of coastal sea areas.
- The proposed activity will demonstrate a better understanding and explanation of meso-scale dynamics and their associated interactions with marine sand waves and spectral wave energy density modulations of short waves at the water surface.
- The previous subject is important for coastal zone management because tidal channels as the Lister Tief show large morphological changes which are hazardous to ship navigation.
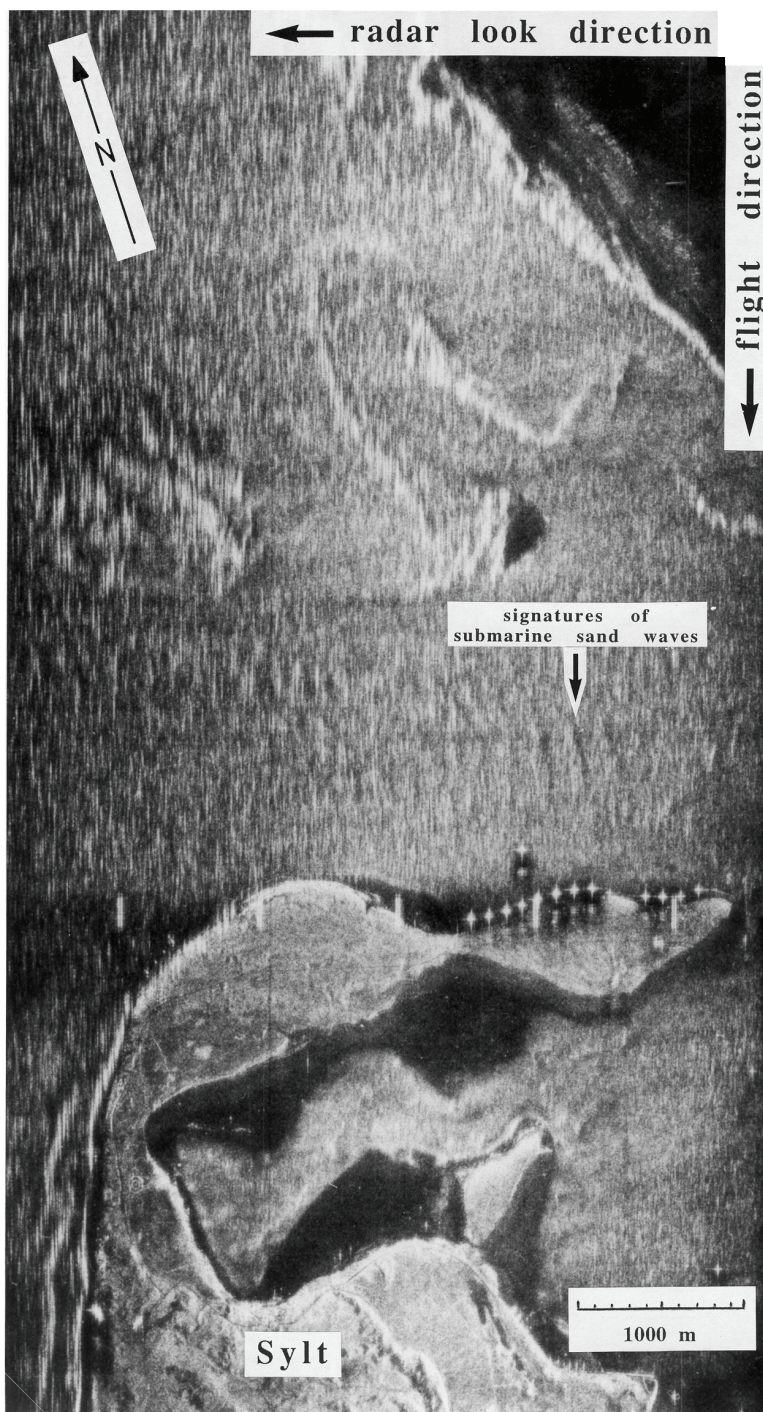

Figure 2: Airborne APD-10 X-band SAR image of subswath B of the Lister Tief taken at 0936 UT 27 September 1979.

Work schedule

The essential task of the project will be the analysis of all TerraSAR-X data as delivered by the DLR. To correctly interprete less well known radar signatures of the coastal zone remotely sensed from space, simultaneous *in situ* data of the sea bed, the water column, and the atmosphere are necessary and will be acquired, processed, combined, and compared with the satellite data. The radar imaging mechanism will be improved by using quasi-specular scattering in combination with the weak hydrodynamic interaction theory. Simulations of NRCS modulation will be carried out and compared with measured TerraSAR-X and RDCP data. An overview of the data interaction scheme is presented in Figure 3.
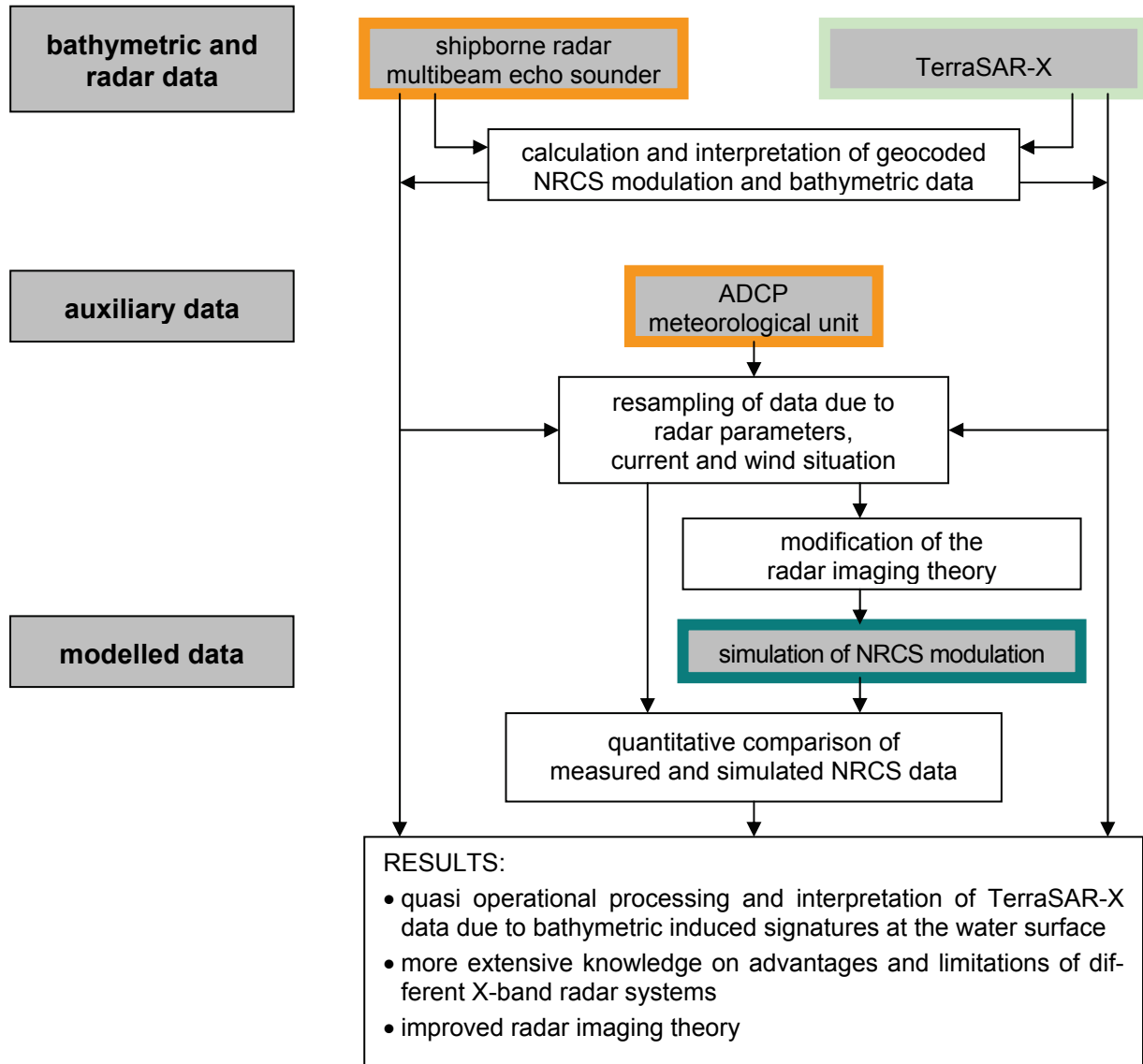
Figure 3: Overview of the data interaction scheme. Original data sets are named by the measuring systems and are colour coded according to the responsible organisation (GKSS: orange, DLR: light green, IFM-GEOMAR: blue green).

METHODS

Study area

The study area of the Lister Tief located north of the island of Sylt is shown in Figure 4. This tidal channel is an ideal test site because of large morphological changes of the sea bed due to strong tidal current velocities. Therefore, the sea area is of permanent interest for coastal zone manage-

ment. Within an area of only 6 km² a complex configuration of different bedforms is found. The sand waves investigated in this tidal channel are four-dimensional in space and time and have heights ≤ 11 m and widths ≤ 300 m. The migration rate of the sand waves is ≤ 80 m per year. Small-scale ripples as well as megaripples of widths ≤ 20 m are superimposed on the larger-scale sand waves. In the Lister Tief the interaction of sea bottom topography, current velocity and sea surface can be described by the so called "kolk-boil" mechanism. A strong kolk is a slowly rotating, upward-tilting vortex on the stoss face of a submarine bedform. It may reach the water surface, can create a cloudy columnar sediment-fluid mixture, and form a raised circular or oval patch at the air-water interface, referred to as a boil. These boils have horizontal scales between 5 m and 25 m in the Lister Tief and are comparable to the flow depth itself as a first approximation. The kolk-boil mechanism is visualised by local and space dependant wave steepening at the sea surface. These so called "waterspouts" are the upward orientated components u_{vert} of the three-dimensional current velocity field measured at the stoss faces of asymmetric marine sand waves. Until now, only two-dimensional profiles of the current velocity as a function of water depth have been analysed in the Lister Tief.
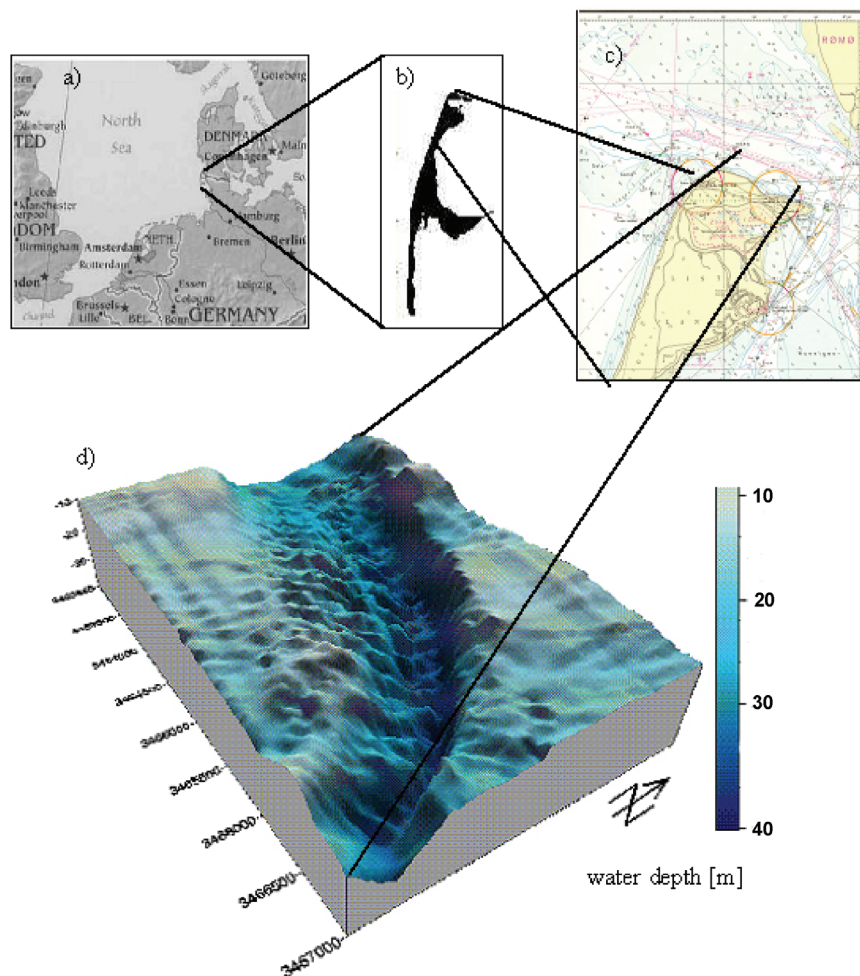

Figure 4: a-c) Locations of the island of Sylt and the Lister Tief in the German Bight of the North Sea; d) Three-dimensional view of the sea bottom topography in the Lister Tief presented on a spatial grid of 20 m × 20 m. Water depths are shown in the range of 8 m (bright blue) to 40 m (dark blue).

Time, radiometric, and spatial resolution of available spaceborne imaging radars of ERS-1/2, RADARSAT, and ENVISAT ASAR have been considered as too low to investigate radar signatures in detail based on the scales described above and associated with meso-scale processes. To map the transport characteristics of these bedforms, satellite- and shipborne radar imaging systems of up to 1 m spatial and up to 1.5 dB radiometric resolution, respectively, are needed. It is expected, that TerraSAR-X will satisfy these requirements. With a scene area of 5 km in azimuth and 10 km

in ground range direction the whole tidal channel of the Lister Tief will be imaged during one over-flight. For the first time, it is expected that the upward orientated vortex cells manifestated as boils at the water surface can be detected from space relative to the orientation of sand wave crests.

Satelliteborne TerraSAR-X measurements

The TerraSAR-X HS data products with a repeat cycle of 11 days will be preprocessed as NRCS modulation data by using commercial software packages of Interactive Data Language (IDL) and adopting new reading, analysis and graphic software of our own. The NRCS modulation data will be visualised as two-dimensional maps. Methods of texture analysis and pattern recognition will be applied and modified for the interpretation of radar signatures. Especially all expected sand wave related phenomena will be analysed. The radar maps as well as selected one-dimensional NRCS modulation profiles will be resampled with respect to wind velocity, tidal current velocity, radar inci-dence angle, and radar look direction, respectively. These resampled data will be used for under-standing the radar imaging mechanism (see section on quasi-specular scattering theory). The comparison of quasi-simultaneously acquired space- and shipborne radar data will provide addi-tional data for validation of the theory. A sufficiently large data set is needed to determine the mi-gration rate of marine sand waves. TerraSAR-X data of a period of at least two years will be proc-essed.

Figure 5 shows the proposed measurement configuration, the TerraSAR-X imaging geometry in spot-light mode, and a schematic sketch of the characteristic fluid flow in the water column, as well as the macroturbulence mechanism caused by ebb tidal currents over flood tide oriented marine sand waves.

Figure 5: Proposed measurement configuration, TerraSAR-X imaging geometry in spotlight mode, and a schematic sketch of the characteristic fluid flow in the water column, the macroturbulence mechanism caused by ebb tidal currents over flood tide oriented marine sand waves, as well as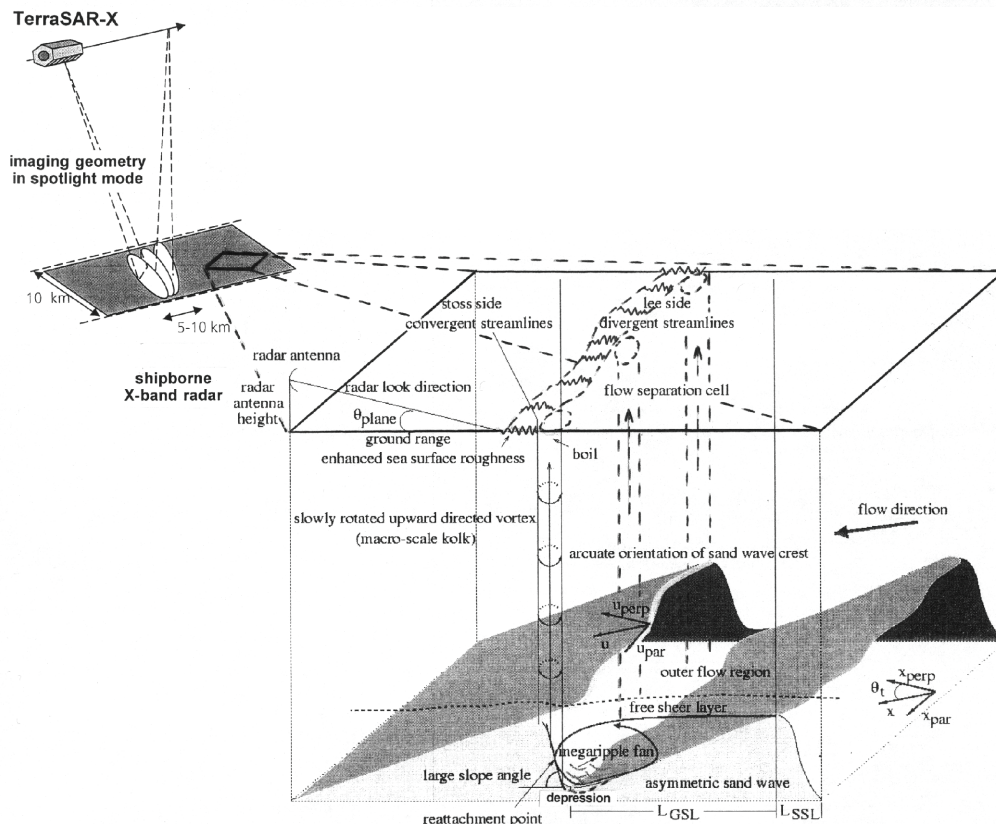 coordinate systems and definition of symbols defined for the investigations which will be carried out in the Lister Tief of the German Bight in the North Sea.

In situ data

In situ data of meteorological and oceanographic parameters will be measured from on board the R.V. *Ludwig Prandtl* during at least two experiments of two weeks duration in the Lister Tief within acquisition times of TerraSAR-X. In addition, video and handheld camera images of the sea surface will be taken during the experiments for interpretation. A moored wave rider buoy measuring the significant wave height, the peak wave period, and the wave travel direction will be also available during the experiments.

Bathymetric measurements

The test site will be surveyed using tracks of 15 m distance. The data gathered by the multibeam echosounder system EM3002 (working frequency 300 kHz, transmitting angle 120°, 160 single depth values) and a Precise Differential Global Positioning System (PDGPS) will be combined and processed as tidal corrected bathymetric data with a spatial resolution of less than 1 m. To compensate the ship motions and the influence of water density stratification, a motion sensor and a Conductivity-Temperature-Depth (CTD) probe will be integrated in the system. The corrected data will be visualised as one-dimensional profiles and as two- and three-dimensional maps. The migration rate of selected sand waves will be determined and semi-yearly depth charts of the period between 2002-2004 will be used as reference data. The yearly achieved bathymetric maps will be the base for the interpretation of space- and shipborne radar data.

Shipborne X-band radar measurements

During the experiments in the Lister Tief two separate X-band radars of the RDCP system on board the R.V. *Ludwig Prandtl* will measure the NRCS. The data of each single radar will be processed as NRCS modulation data. These shipborne radar data will then be analysed using the same methods as applied for the TerraSAR-X NRCS modulation data (see section on satellite-borne TerraSAR-X measurements). The data of both shipborne radars will be merged, geocoded, and processed as surface current vectors. In the final data processing step the surface current gradient of these data will be calculated and visualised in geocoded maps. As one of the most important parameters of the radar imaging mechanism these surface current gradients will be used for simulations of the NRCS modulation of the improved quasi-specular scattering theory (see section on quasi-specular scattering theory).

Acoustic Doppler Current Profiler (ADCP) measurements

To analyse the change of the current velocity in horizontal as well as in vertical direction depending on water depth, at least one ADCP data set using measurements from on board the R.V. *Ludwig Prandtl* during ebb tidal phase and flood tidal phase, respectively, will be derived and processed as three-dimensional maps. The waterspouts associated with the boils at the water surface will be identified in relation to the sand wave orientation and will be compared with radar signatures detected by TerraSAR-X. Expected relationships between TerraSAR-X signatures and the slope as well as the three-dimensional shape of the sand wave will be investigated.

Meteorological measurements

To confirm the assumed dependence of NRCS modulation at the water surface on the angle between the wind- and current direction, particularly at low grazing angle radar illumination, also meteorological parameters will be acquired. During the project the wind speed and -direction will be measured continuously at the shore station of the northern part of the island of Sylt which is operated by the GKSS Research Centre. During the ship campaigns in the Lister Tief the wind speed and -direction will also be measured from on board the R.V. *Ludwig Prandtl*. The TerraSAR-X and shipborne X-band NRCS modulation data due to marine sand waves will be analysed as a function of wind speed and -direction. In addition, the NRCS modulation data will also be analysed as a function of the radar look direction relative to the wind direction and the local current direction, respectively. The wind speed and -direction are needed as input data for simulations of the NRCS modulation.

QUASI-SPECULAR SCATTERING THEORY

Specular reflection occurs when radiation is scattered into a given direction from surface regions with slopes such that the local specular direction coincides with the scattering direction. The quasi-specular scattering theory can be applied if the wavelengths of waves in the ocean contributing to the mean square surface slope are larger than the wavelength of the microwave. In general, the mean squared slope of such waves is small. But this is considerably different if waves are influenced by a surface current gradient. Very steep disturbed slopes of the order of 10° or more can arise in the converging zone of the current correlated with the slope regions of marine sand waves. Especially trochoidal shapes of water waves can be generated due to such a kind of wave-current interaction at low to moderate wind speeds. These trochoidal shaping waves are producing an ensemble average of facets which create quasi perpendicular planes relative to the transmitted radar beam. There also exist steep small gravity waves in this zone which tend to become sharp wedges just before they break and breaking waves themselves. Improvements of the quasi-scattering theory have to be made because the radar imaging mechanism of the sea bed also strongly depends on the up- and crosswind wave slopes, the angle between the upwind and perpendicular current direction to the sand wave crest, and the angle between the radar range direction and the upwind direction.

The NRCS σ_0 for finitely conductive rough surfaces based on quasi-specular scattering is given by (18)

$$\sigma_0(\theta_0) = \pi |R(0)|^2 \sec^4\theta_0\, p_0(\zeta_{x0},\zeta_{y0}) \tag{1}$$

where $R(0)$ is the Fresnel reflection coefficient at normal incidence, θ_0 is the angle of incidence, $p_0(\zeta_{x0},\zeta_{y0})$ is the background joint-probability density of slopes of the vertical elevation of the sea surface ζ_0, $\zeta_{x0} = \partial\zeta_0/\partial x$ and $\zeta_{y0} = \partial\zeta_0/\partial y$ are the slopes of the rough sea surface in two orthogonal directions, x and y. For an isotropic rough ocean surface obeying Gaussian statistics according to the incident angle dependence for quasi-specular scattering Eq. (1) is rewritten as

$$\sigma_0(\theta_0) = \pi \frac{|R(0)|^2}{s_0^2} \sec^4\theta_0 \exp\left(-\frac{\tan^2\theta_0}{s_0^2}\right) \tag{2}$$

where s_0^2 is the total variance of slopes created by the ocean waves. Eq. (2) has been used as a first-order theory by (14) for simulations of the NRCS modulation due to quasi-specular scattering at very low grazing angle illumination caused by marine sand waves.

The following proposed improved quasi-scattering theory contains the additional influence of the up- and crosswind wave slopes, the angle between the upwind and perpendicular current direction to the sand wave crest, and the angle between the radar range direction and the upwind direction (see also Figure 5). At short radar wavelengths, the probability density distribution function for sea surface slopes published by (19) will be used here. It has been shown by (19) that the probability density distribution of surface wave slopes, $p_0(\varsigma_{x0},\varsigma_{y0})$ (see Eq. (1)), is a Gram-Charlier series (20) with a variance of wave slopes depending on wind speed and direction. This distribution can be expressed as

$$
\begin{aligned}
p_0(\zeta_{x0},\zeta_{y0}) \approx {} & \frac{1}{2\pi\sigma_{u0}\sigma_{c0}}\left\{\exp\left[-\frac{1}{2}\left(s_{u0}^2 + s_{c0}^2\right)\right]\right\} \\
& \left\{1-\left(\frac{1}{2}\right)c_{21}\left(s_{c0}^2 - 1\right)\right. \\
& -\left(\frac{1}{6}\right)c_{03}\left(s_{u0}^3 - 3s_{u0}\right)+\left(\frac{1}{4}\right)c_{22}\left(s_{c0}^2 - 1\right)\left(s_{u0}^2 - 1\right) \\
& \left.+\left(\frac{1}{24}\right)\left[c_{40}\left(s_{c0}^4 - 6s_{c0}^2 + 3\right)+c_{04}\left(s_{u0}^4 - 6s_{u0}^2 + 3\right)\right]\right\}
\end{aligned}
\tag{3}
$$

where the leading term on the right hand side of expression (3) represents a Gaussian distribution as shown above by Eq. (2). The squared normalised background upwind and crosswind slope are defined as

$$s_{u0}^2 = \frac{\zeta_{x0}^2}{\sigma_{u0}^2} \qquad (4a)$$

and

$$s_{c0}^2 = \frac{\zeta_{y0}^2}{\sigma_{c0}^2} \qquad (4b)$$

The variances of the background upwind and crosswind slope are given by

$$\sigma_{u0}^2 = a + b u_w \qquad (5a)$$

and

$$\sigma_{c0}^2 = c + d u_w \qquad (5b)$$

where u_w is the wind speed. The skewness coefficients are expressed by

$$c_{21} = e - f u_w \qquad (6a)$$

and

$$c_{03} = g - h u_w \qquad (6b)$$

The values for the coefficients in these relationships are given in Table 2 (19).

Table 2: Parameters in slope probability density distribution published by (19) (all quantities have to be multiplied by 10^{-3}).

Parameter	Symbol	Clean Surface	Slick Surface
Upwind coefficients	a	0.0	5.0
	b	3.16	0.78
Crosswind coefficients	c	3.0	3.0
	d	1.92	0.84
Skewness coefficients	e	10.0	0.0
	f	8.6	0.0
	g	40.0	20.0
	h	33.0	0.0
Peakedness coefficients	c_{40}	400.0	360.0
	c_{22}	120.0	100.0
	c_{04}	230.0	260.0

Rewriting ς_x, ς_y, σ_u^2, σ_c^2, and θ as sums of a constant equilibrium term and a time-dependent perturbation term, respectively, yields

$$\zeta_x = \zeta_{x0} + \delta\zeta_x \qquad (7a)$$

$$\zeta_y = \zeta_{y0} + \delta\zeta_y \qquad (7b)$$

$$\sigma_u^2 = \sigma_{u0}^2 + \delta\sigma_u^2 \qquad (8a)$$

$$\sigma_c^2 = \sigma_{c0}^2 + \delta\sigma_c^2 \qquad (8b)$$

and

$$\theta = \theta_0 + \delta\theta \qquad (9)$$

The incidence angle for a plane sea surface θ_0 in Eq. (1) and (9), respectively, is now redefined as the effective incidence angle θ_0 for a real sea surface with roughness

$$\theta_0 = \theta_{plane} + \theta_{rough} \qquad (10)$$

where θ_{plane} is the incidence angle for a plane surface. The tangent square of the incidence angle of the background rough sea surface as a function of u_w has been derived by (19) as

$$\tan^2\theta_{rough} = s_0^2 = \langle \zeta_{x0}^2 \rangle + \langle \zeta_{y0}^2 \rangle = 0.003 + 0.0051 u_w \pm 0.004 \tag{11}$$

The local normalised upwind and crosswind slope are defined by

$$s_u^2 = \frac{\left(\zeta_{x0}^2 + \delta\zeta_x^2\right)}{\left(\sigma_{u0}^2 + \delta\sigma_u^2\right)} \tag{12a}$$

and

$$s_c^2 = \frac{\left(\zeta_{y0}^2 + \delta\zeta_y^2\right)}{\left(\sigma_{c0}^2 + \delta\sigma_c^2\right)} \tag{12b}$$

where

$$\zeta_{x0} = -\tan\theta_0 \cos\varphi \tag{13a}$$

and

$$\zeta_{y0} = -\tan\theta_0 \sin\varphi \tag{13b}$$

with the angle φ between the radar range direction and the upwind direction and

$$\delta\zeta_x = -\tan\delta\theta \cos\varphi \tag{14a}$$

and

$$\delta\zeta_y = -\tan\delta\theta \sin\varphi \tag{14b}$$

Assuming that the time-dependent perturbation terms in Eqs. (7)-(9) caused by the disturbance of the surface current $\delta U(\vec{x})$ due to marine sand waves obey also a Gram-Charlier series as defined by Eq. (3), then the disturbed NRCS $\delta\sigma$ is given by

$$\delta\sigma = \sigma - \sigma_0 = \pi|R(0)|^2 \sec^4(\theta_0 + \delta\theta) p(\zeta_{x0} + \delta\zeta_x, \zeta_{y0} + \delta\zeta_y) - \sigma_0 \tag{15}$$

where σ is the local NRCS influenced by the disturbance of $\delta U(\vec{x})$.

The local joint-probability density function of slopes is now defined by

$$p(\zeta_{x0} + \delta\zeta_x, \zeta_{y0} + \delta\zeta_y) \approx \frac{1}{2\pi\sigma_u\sigma_c}\left\{\exp\left[-\frac{1}{2}\left(s_u^2 + s_c^2\right)\right]\right\}$$
$$\left\{1 - \left(\frac{1}{2}\right)c_{21}\left(s_c^2 - 1\right)\right.$$
$$\left. - \left(\frac{1}{6}\right)c_{03}\left(s_u^3 - 3s_u\right) + \left(\frac{1}{4}\right)c_{22}\left(s_c^2 - 1\right)\left(s_u^2 - 1\right)\right.$$
$$\left. + \left(\frac{1}{24}\right)\left[c_{40}\left(s_c^4 - 6s_c^2 + 3\right) + c_{04}\left(s_u^4 - 6s_u^2 + 3\right)\right]\right\} \tag{16}$$

The tangent square of the disturbed incidence angle is derived by

$$\tan^2\delta\theta = +\delta\sigma^2 = \delta\sigma_u^2 + \delta\sigma_c^2 \quad, \quad \frac{\partial u_{perp}}{\partial x_{perp}} \le 0 \tag{17a}$$

and

$$-\tan^2\delta\theta = -\delta\sigma^2 = -\left(\delta\sigma_u^2 + \delta\sigma_c^2\right) \quad, \quad \frac{\partial u_{perp}}{\partial x_{perp}} > 0 \tag{17b}$$

with

$$\delta\sigma_u^2 = \int_{k_0}^{k_c} \vec{k}^2(\vec{x})\delta F(\vec{x},\vec{k})\cos\alpha \, d\vec{k} \tag{18a}$$

and
$$\delta\sigma_c^2 = \int_{k_0}^{k_c} \vec{k}^2(\vec{x})\,\delta F(\vec{x},\vec{k})\sin\alpha\ \mathrm{d}\vec{k} \tag{18b}$$

where x_{perp} is the space variable defined perpendicular to the sand wave crest, $\vec{k}$ is the wave number vector of short gravity waves, k_0 is the lower limit of the wave number producing quasi-specular scattering modulation, k_c is the maximum wave number neglecting the effect of surface tension, $\partial u_{\mathrm{perp}} / \partial x_{\mathrm{perp}}$ is the gradient or strain rate of the current velocity perpendicular to the sand wave crest, α is the angle between the upwind direction and the current velocity component perpendicular to the sand wave crest, and $\delta F(\vec{x},\vec{k})$ is the perturbation term of the wave-energy density spectrum in the short gravity wave regime caused by wave-current interaction applying the weak hydrodynamic interaction theory (21).

The relationship between $\Psi(\vec{k})$, $F(\vec{k})$ and the wave action density spectrum $N(\vec{k}) = F(\vec{k})(\omega'(k))^{-1}$ is defined by (8)

$$F(\vec{k}) = \omega'(k)N(\vec{k}) = \frac{\omega'(k)^2}{k}\psi(\vec{k}) \tag{19}$$

with the wave height spectrum
$$\psi(k) = a_p k^{-4} \tag{20}$$

where a_P is known as the Phillips constant. Based on measurements by (22), the empirical relation for a_P as a function of wind speed $u_w \le 8\ \mathrm{m\ s^{-1}}$ is used

$$\log_{10}a_p = -2.90 + 3.06\cdot 10^{-1}u_w - 1.85\cdot 10^{-2}u_w^{\ 2} \tag{21}$$

The dispersion relation for gravity waves in Eq. (19) is defined by

$$\omega' = (gk)^{1/2} \tag{22}$$

For the modulation of the first order perturbed wave-energy density spectrum $\delta F / F_0 = (F - F_0)/F_0$ (with F_0 as the unperturbed wave-energy density spectrum) the expression derived by (4) is used

$$\frac{\delta F}{F_0} = -4.5\frac{\partial u_{\mathrm{perp}}}{\partial x_{\mathrm{perp}}}\left(\left(\vec{c_g} + \vec{u_0}\right)\frac{1}{L} + \mu\right)^{-1} \tag{23}$$

with the absolute value of the group velocity for gravity waves

$$\left|\vec{c}_g\right| = \frac{1}{2}\frac{\omega'}{k} \tag{24}$$

where $\vec{u}_0$ is the mean current velocity of the undisturbed sea area, μ is the relaxation rate parameter, g is the acceleration of gravity, L = L_{SSL} is the length scale of the steep slope, and L = L_{GSL} is the length scale of the gentle slope of the sand wave, respectively.

More information of the weak hydrodynamic interaction theory for the radar imaging mechanism of the sea bed is given in (4) and (14). The quasi-specular scattering theory as outlined above will be applied and tested for the TerraSAR-X incidence angle of 55° in order to explain the NRCS modulation caused by marine sand waves. Simulations of the NRCS modulation due to quasi-specular scattering caused by marine sand waves will be carried out as a function of radar incidence angle, radar look direction, tidal current speed and -direction, and wind speed and -direction, respectively. The simulations will be analysed and compared with satelliteborne TerraSAR-X data and shipborne X-band radar data.

CONCLUSIONS

The main objective of the described project is the high potential in the scientific evaluation of TerraSAR-X data especially for coastal waters. It is expected that the very high geometric and radiometric resolution of TerraSAR-X enables a very detailed analysis of sea bottom topography signatures at the water surface. For the first time, it will be possible from space to identify NRCS modulations caused by meso-scale sand waves ≤ 300 m widths at water depths ≤ 40 m. Often, unique oceanographic phenomena such as up- and downwelling events, turbulence, and eddies are associated with marine sand waves in the tidal channel of the Lister Tief. The interaction of hydro-, sediment- and morphodynamics in tidal channels covered by four-dimensional bedforms in time and space is not well understood and has to be improved by using TerraSAR-X data. Shipborne X-band radar data and *in situ* bathymetric measurements as well as meteorological and current velocity data will be also available during the project and are essential for the interpretation of the TerraSAR-X data. An improved radar imaging theory based on quasi-specular scattering has been introduced here and will be tested by simulations of the NRCS modulation and compared with TerraSAR-X as well as shipborne radar data. The proposed research offers good potentials to apply radar remote sensing techniques to coastal zone management and rapid synoptic surveying.

REFERENCES

1　Lamprecht H-O, 1957. Uferveränderungen und Küstenschutz auf Sylt. Die Küste, 6: 39-93

2　Kelletat D, 1992. Coastal erosion and protection measures at the German North Sea coast. Journal of Coastal Research, 8: 699-711

3　Valenzuela G R, 1978. Theories for the interaction of electromagnetic and ocean waves - A review. Boundary-Layer Meteorology, 13: 277-293

4　Alpers W & I Hennings, 1984. A theory of the imaging mechanism of underwater bottom topography by real and synthetic aperture radar. Journal of Geophysical Research, 89(C6): 10529-10546

5　Phillips O M, 1984. On the response of short ocean wave components at a fixed wavenumber to ocean current variations. Journal of Physical Oceanography, 14: 1425-1433

6　Shuchman R A, D R Lyzenga & G A Meadows, 1985. Synthetic aperture radar imaging of ocean-bottom topography via tidal-currents interactions: theory and observations. International Journal of Remote Sensing, 6: 1179-1200

7　Zimmerman J F T, 1985. Radar images of the sea bed. Nature, 314: 224-226

8　Holliday D, G St-Cyr & N E Woods, 1986. A radar ocean imaging model for a small to moderate incidence angles. International Journal of Remote Sensing, 7: 1809-1834

9　Van Gastel K, 1987. Imaging by X band radar of subsurface features: a nonlinear phenomenon. Journal of Geophysical Research, 92(C6): 11957-11865

10　Romeiser R & W Alpers, 1997. An improved composite surface model for the radar backscattering cross section of the ocean surface. 2. Model response to surface roughness variations and the radar imaging of underwater bottom topography. Journal of Geophysical Research, 102(C6): 25251-25267

11　Vogelzang J, 1997. Mapping submarine sandwaves with multi-band imaging radar 1. Model development and sensitivity analysis. Journal of Geophysical Research, 102(C6): 1163-1181

12　Inglada J & R Garello, 2002. On rewriting the imaging mechanism of underwater bottom topography by synthetic aperture radar as a Volterra series expansion. IEEE Journal of Oceanic Engineering, 27: 665-674

13　Lamont-Smith T, A M Jackson, P W Shepherd & R D Hill, 2005. Low grazing angle radar imaging experiments over the South Falls sandbank. International Journal of Remote Sensing, 26: 937-966

14 Hennings I & D Herbers, 2006. Radar imaging mechanism of marine sand waves at very low grazing angle illumination caused by unique hydrodynamic interactions. Journal of Geophysical Research, 111: C10008, doi:10.1029/2005JC003302

15 Marghany M & M Hashim, 2006. Three-dimensional reconstruction of bathymetry using C-band TOPSAR data. Photogrammetrie Fernerkundung Geoinformation, 6/2006: 469-480

16 Hennings I, D Herbers, K Prinz & F Ziemer, 2004. First results of the OROMA experiment in the Lister Tief of the German Bight in the North Sea. EARSeL eProceedings, 3: 86-104

17 Gargett A, J Wells, A E Tejada-Martinez & C E Grosch, 2004. Langmuir supercells: a mechanism for sediment resuspension and transport in shallow seas. Science, 306: 1925-1928

18 Barrick D E, 1968. Rough surface scattering based on the specular point theory. IEEE Transactions on Antennas and Propagation, AP-16: 449-454

19 Cox C & W Munk, 1954. Measurement of the roughness of the sea surface from photographs of the sun's glitter. Journal of the Optical Society of America, 44: 838-850

20 Trueblood K N, H-B Bürgi, H Burzlaff, J D Dunitz, C M Gramaccioli, H H Schulz, U Shmueli & S C Abrahams, 1996. Atomic displacement parameter nomenclature. Acta Crystallographica, A52: 770-781

21 Alpers W & K Hasselmann, 1978. The two-frequency microwave technique for measuring ocean wave spectra from an airplane or satellite. Boundary-Layer Meteorology, 13: 215-230

22 Stolte S, 1990. Dynamics of short waves and wave breaking (Federal Armed Forces Underwater Acoustics and Marine Geophysics Research Institute Kiel) Report 1990-4, 48 pp.